Isotope-production cross sections of residual nuclei in proton- and deuteron-induced reactions on ^{93}Zr at 50 MeV/u

Keita Nakano[1,2,*], *Yukinobu* Watanabe[1], *Shoichiro* Kawase[1], *He* Wang[2], *Hideaki* Otsu[2], *Hiroyoshi* Sakurai[2], *Nobuyuki* Chiga[2], *Junki* Suwa[1,2], *Toshiyuki* Sumikama[2], *Satoshi* Takeuchi[3], *Takashi* Nakamura[3], *Kazuya* Chikaato[4], *Maya* Takechi[4], *Shunpei* Koyama[5], *Deuk Soon* Ahn[2], *Hidetada* Baba[2], *Sidong* Chen[2], *Martha Liliana* Cortes[2], *Pieter* Doornenbal[2], *Naoki* Fukuda[2], *Akihiro* Hirayama[3], *Ryohei* Hosoda[4], *Tadaaki* Isobe[2], *Shunsuke* Kawakami[6], *Yosuke* Kondo[3], *Shigeru* Kubono[2], *Yukie* Maeda[6], *Shoichiro* Masuoka[7], *Shin'ichiro* Michimasa[7], *Ian* Murray[2], *Ryo* Nakajima[7], *Megumi* Niikura[5], *Tomoyuki* Ozaki[3], *Atsumi* Saito[3], *Takeshi* Saito[5], *Hiromi* Sato[2], *Yohei* Shimizu[2], *Susumu* Shimoura[7], *Yoshiki* Soudo[6], *Pär-Anders* Söderström[2], *Xiaohui* Sun[2], *Daisuke* Suzuki[2], *Hiroshi* Suzuki[2], *Hiroyuki* Takeda[2], *Yasuhiro* Togano[3], *Takato* Tomai[3], *Hiroki* Yamada[3], *Masahiro* Yasuda[3], and *Koichi* Yoshida[2]

[1]Department of Advanced Energy Engineering Sciences, Kyushu University, 6-1 Kasuga-koen, Kasuga, Fukuoka 816-8580, Japan
[2]RIKEN Nishina Center, 2-1 Hirosawa, Wako, Saitama 351-0198, Japan
[3]Department of Physics, Tokyo Institute of Technology, 2-12-1 Ookayama, Meguro, Tokyo 152-8551, Japan
[4]Graduate School of Science and Technology, Niigata University, 8050 Ikarashi 2-no-cho, Nishi-ku, Niigata 950-2181, Japan
[5]Department of Physics, University of Tokyo, 7-3-1 Hongo, Bunkyo, Tokyo 113-0033, Japan
[6]Faculty of Engineering, University of Miyazaki, 1-1 Gakuen Kibanadai-nishi, Miyazaki, Miyazaki 889-2192, Japan
[7]Center for Nuclear Study, University of Tokyo, 2-1 Hirosawa, Wako, Saitama 351-0198, Japan

Abstract. The isotope-production cross sections in *p*- and *d*-induced reactions on ^{93}Zr at approximately 50 MeV/nucleon were measured by using the inverse-kinematics method at RIKEN RI Beam Factory. The measured data were compared with the previous experimental ^{93}Zr + *p*, *d* at 105 and 209 MeV/nucleon data. This comparison represents that the isotopic distribution of production cross sections at 51 MeV *p*-induced reaction is appreciably different from those at 105 and 209 MeV. On the other hand, these three data sets show that the shape of isotopic distribution is similar in the case of the *d*-induced reaction. Also, the measured production cross sections were compared with the theoretical model calculations with Particle and Heavy Ion Transport code System (PHITS) version 3.10 in order to investigate the reproducibility of the models implemented in PHITS. The calculations well reproduced the experimental data even in such low incident energy, while several discrepancies were still seen as in the *p*- and *d*-induced reactions at 105 and 209 MeV/nucleon.

1 Introduction

The treatment of high-level radioactive waste (HLW) is one of the crucial issues concerning nuclear power generation. The geological disposal has been advanced as the first candidate for the option of its disposal, however there is still the risk of long-term radiotoxicity. To resolve this situation, nuclear transmutation has been proposed as a powerful tool to give a new option for the HLW disposal for the last several decades. In recent years, a series of nuclear data measurements for long-lived fission products (LLFPs) has been performed in Japan in order to accumulate the basic data necessary to design nuclear transmutation system for LLFPs [1–6]. Isotope-production cross sections in *p*- and *d*-induced reactions on ^{93}Zr, which is a typical LLFP with its half-life of 1.5×10^6 years, have been measured at the reaction energies of 105 and 209 MeV/nucleon, and theoretical model analyses with the intra-nuclear cascade model and evaporation model have been performed so far [1, 2]. As a next step, it is of our interest to investigate the incident energy dependence of isotopic distribution of production cross sections by further measurements in the lower incident energy region where the spallation reaction is no more dominant.

In the present work, isotope-production cross sections for ^{93}Zr were measured at the reaction energy of approximately 50 MeV/nucleon using the inverse-kinematics method. The measured cross sections are compared with those measured previously at 105 and 209 MeV/nucleon, and the incident energy dependence of isotopic distributions is discussed. In addition, theoretical model calculations are compared with the measured data for benchmarking of the models in the low incident energy region.

2 Experiment

The experiment was performed at RIKEN RI Beam Factory (RIBF). The BigRIPS RI beam separator was used for separation and identification of the secondary beam, and ZeroDegree Spectrometer (ZDS) was used for identification of the reaction products [7].

*e-mail: knakano@aees.kyushu-u.ac.jp

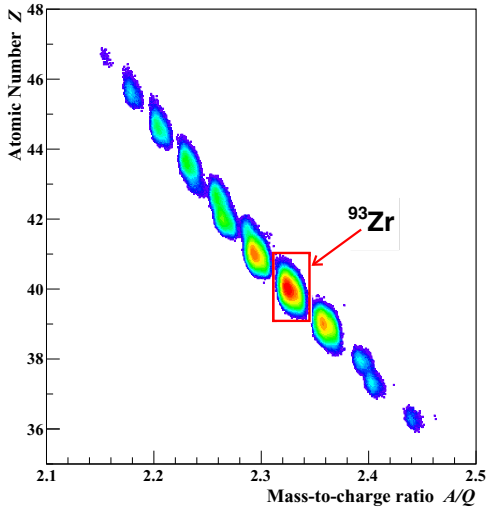

Figure 1. Particle identification plot for the secondary beam. The red box outlines the ^{93}Zr beam.

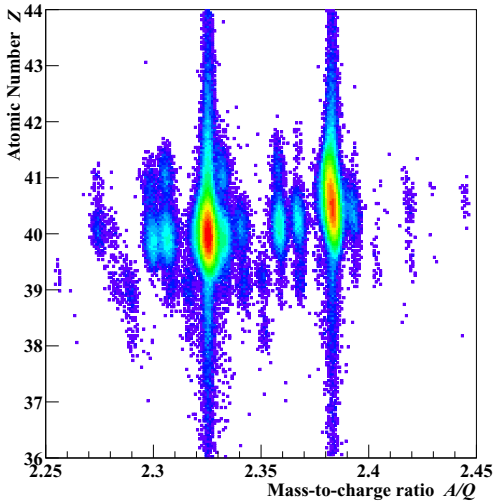

Figure 2. Particle identification plot for reaction products from the H_2 target after selecting the ^{93}Zr beam.

First, an accelerated ^{238}U primary beam up to 345 MeV/nucleon impinged onto a 3-mm-thick ^{9}Be production target located at the entrance of BigRIPS to produce the secondary cocktail beam via the in-flight fission. Next, the secondary beam was purified and identified via the TOF$-B\rho-\Delta E$ method [8] at the first- and second-halves of BigRIPS, respectively. Figure 1 shows a two-dimensional identification plot for the secondary beam by the atomic number Z and the mass-to-charge ratio A/Q, and ^{93}Zr was clearly identified. The purity and typical count rate of ^{93}Zr were 57.8% and 980 count per second, respectively.

Then the secondary beam impinged onto the reaction targets. As the reaction targets, cooled H_2 and D_2 gases pressurized to 4 atm were used. The thicknesses of H_2 and D_2 gases were 20.2 and 34.5 mg/cm^2, respectively. The incident energy of ^{93}Zr was 51 MeV/nucleon at the center of the H_2 target and was 52 MeV/nucleon at the center of the D_2 target. The reaction products were also identified at ZDS using a method similar to that for the secondary beam. To cover the wide range of produced isotopes, nine different $B\rho$ settings for ZDS were adopted. Figure 2 represents the identification plot for the reaction products from the H_2 reaction target. Since the fragments have lower kinetic energy than those in the previous measurements [1, 2], they easily pick up electrons and change their charge states. As a result, reaction products with a few charge states, *i.e.*, fully-stripped, hydrogen-like, and helium-like fragment, were observed in Fig. 2. The isotope-production cross section for each reaction product was derived from the yields of incident ^{93}Zr beam and each isotope produced with each charge state by subtracting the contribution from beamline materials which can be estimated by the empty target runs.

3 Results and Discussion

The red circles in Figs. 3 and 4 show the measured isotope-production cross sections for the p-induced reaction at 51 MeV (σ_{p51}) and the d-induced reaction at 52 MeV/nucleon (σ_{d52}) on ^{93}Zr, respectively. The error bars indicate the statistical uncertainties. The σ_{p51} and σ_{d52} data were obtained for 17 and 20 nuclides, respectively. It should be emphasized that the inverse-kinematics enables us to obtain systematic isotope-production data including not only short-lived nuclei but also stable ones.

3.1 Energy dependence

The isotope-production cross sections measured in the present work were compared with the previous experimental data in order to investigate the energy dependence of isotope production. The previously measured data at 105 and 209 MeV/nucleon [1, 2] are displayed by the black triangles (σ_{p105} and σ_{d105}) and the blue squares (σ_{p209} and σ_{d209}) in Figs 3 and 4, respectively.

Four following differences are observed among the three data sets. To begin with, in Fig. 3 (b) and (c), the lower mass limits of σ_{p51} distribution end at larger mass number than those of σ_{p105} and σ_{p209}, resulting in the narrow distribution. The measured range of the cross section is restricted by the lower limit of measurable cross section and by the acceptance of ZDS. Since incident particle with higher kinetic energy can remove more nucleons than that with lower kinetic energy, the isotopic distribution of σ_{p51} has such a narrower range than the previous data. Next, σ_{p51} have much larger production cross sections near the target nucleus ^{93}Zr. These nuclei are mainly produced via the fusion-evaporation process where incident particle is captured by the target nuclei and subsequently deexcited with emission of several particles. In the lower incident energy case, such process is largely enhanced. As a result, Nb and Zr isotopes with large-mass number have much larger cross sections than those in the higher incident energy cases. Then, in Fig. 3 (c), σ_{p51} for Y isotopes show a very different trend from σ_{p105} and σ_{p209}. In particular, ^{87}Y has quite large production cross section in σ_{p51}, and the unique behavior is observed in the Y isotopic chain.

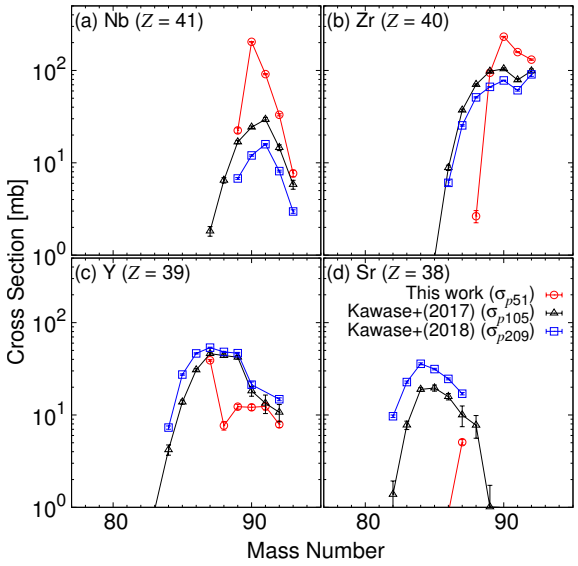

Figure 3. The measured isotope-production cross sections for p-induced reaction on ^{93}Zr at 51 MeV with previous works at 105 and 209 MeV.

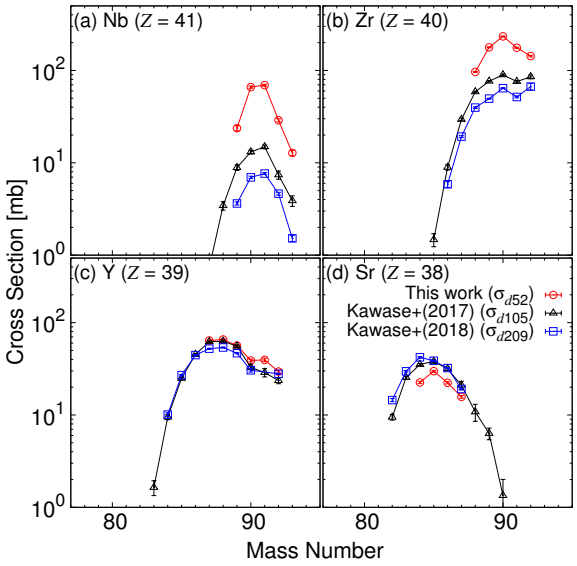

Figure 4. The same as Fig. 3, but for d-induced reaction at 52 MeV/nucleon with previous works at 105 and 209 MeV/nucleon.

This indicates that the production of ^{87}Y is enhanced in the incident energy of around 50 MeV. Finally, in the previous data, the productions of ^{90}Zr and ^{89}Y were enhanced due to closed shell effect at the neutron magic number $N = 50$, resulting in discontinuous jumps at ^{90}Zr and ^{89}Y. Although isotopic distribution of Zr shows a jump between ^{90}Zr and ^{91}Zr, no clear jump is seen in Y isotopes regardless of the presence of jumps in σ_{p105} and σ_{p209}.

As for the d-induced reaction shown in Fig. 4, the distributions of σ_{d52}, σ_{d105}, and σ_{d209} have similar shape. In terms of their quantities, the Nb and Zr isotope-production cross sections decrease with an increase in incident energy. In contrast, Sr isotope-production cross sections increase with an increase in incident energy. As mentioned above, the Nb and Zr isotopes which are near the target nucleus ^{93}Zr are largely produced by the fusion-evaporation process which is dominant in nuclear reactions at lower kinetic energies. On the other hand, the production of Sr isotopes, which requires much particle emissions like a spallation reaction, is enhanced in the higher incident energy cases. As a result, the dependence of isotope-production cross sections on incident energy has a different tendency in each isotopic chain. Finally, these three data sets show jumps at the neutron magic number $N = 50$ in both Zr and Y isotopes.

3.2 Comparison with theoretical calculation

The measured isotope-production cross sections were compared with theoretical model calculations with Particle and Heavy Ion Transport code System (PHITS) version 3.10 [9, 10] as shown in Fig. 5. In the PHITS calculation, the nuclear reaction is assumed to proceed as a two-step process, that is, the intra-nuclear cascade process modeled as incoherent nucleon-nucleon collisions and the evaporation process where pre-fragments deexcite with emitting particles and gamma-rays. The Liège Intranuclear Cascade model (INCL-4.6) [11] and the Generalized Evaporation Model (GEM) [12] were employed for each process to calculate the isotope-production cross section in PHITS. Although INCL-4.6 model was developed for nuclear reactions having the kinetic energy above several hundred MeV, the calculations well predict the measured isotopic distributions of production cross sections even in the 50 MeV/nucleon data. However, they show some discrepancies seen in the 105 and 209 MeV/nucleon cases. First, the calculations are shifted by one-mass number to the heavy side in the distribution of the Nb isotope-production cross sections in both of the p- and d-induced reactions. Next, the calculations overestimate the production cross sections near the target nucleus ^{93}Zr. Also, the exaggerated even-odd staggering is observed in calculated Sr isotopes in the d-induced reaction regardless of weak staggering of the measured data. These discrepancies are also pointed out in the previous studies [1, 2], and they still appear over the range of these incident energy. Finally, the calculated isotopic distribution of Y has a sharp rise seen at the mass number of 87, but underestimates the production cross section.

4 Conclusions

We have measured isotope-production cross sections for p- and d-induced reactions on long-lived fission product ^{93}Zr at approximately 50 MeV/nucleon at RIKEN RIBF. The energy dependence of isotopic distribution of production cross sections were investigated for both of the reactions. In the d-induced reaction, three data sets showed similar tendency but different quantities each other. In the p-induced reaction, in contrast, a narrower distribution was observed in 51 MeV data compared with the higher incident energy cases due to the insufficient

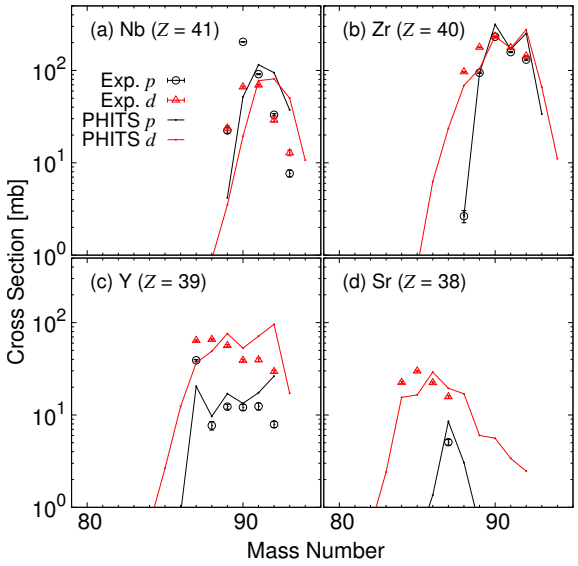

Figure 5. Comparison between the measured isotope-production cross sections and calculated cross sections with PHITS version 3.10 for *p*- and *d*-induced reactions on ^{93}Zr at approximately 50 MeV/nucleon.

energy to knock out and/or emit many nucleons. Also, the measured isotope-production cross sections were compared with the calculations by PHITS version 3.10 employing INCL-4.6 model plus GEM. The comparison represented an overall agreement even in approximately 50 MeV/nucleon case. However, several discrepancies were seen in the present data as in the data measured at 105 and 209 MeV/nucleon. In the future, continuous expansions to wider incident energy ranges will be required especially in lower incident energy such as 30 and/or 20 MeV/nucleon for comprehensive understanding of the reaction process.

Acknowledgment

This work was funded by ImPACT Program of Council for Science, Technology and Innovation (Cabinet Office, Government of Japan). The authors would like to thank the accelerator staff of the RIKEN Nishina Center for providing high-quality ^{238}U primary beam.

References

[1] S. Kawase, K. Nakano, Y. Watanabe, H. Wang, H. Otsu, H. Sakurai, D.S. Ahn, M. Aikawa, T. Ando, S. Araki et al., Progress of Theoretical and Experimental Physics **2017**, 093D03 (2017)

[2] S. Kawase, Y. Watanabe, K. Nakano, J. Suwa, H. Wang, N. Chiga, H. Otsu, H. Sakurai, S. Takeuchi, T. Nakamura et al., JAEA-Conf2018-001 **2018**, 111 (2018)

[3] H. Wang, H. Otsu, H. Sakurai, D.S. Ahn, M. Aikawa, P. Doornenbal, N. Fukuda, T. Isobe, S. Kawakami, S. Koyama et al., Physics Letters B **754**, 104 (2016)

[4] H. Wang, H. Otsu, H. Sakurai, D.S. Ahn, M. Aikawa, T. Ando, S. Araki, S. Chen, N. Chiga, P. Doornenbal et al., Progress of Theoretical and Experimental Physics **2017**, 021D01 (2017)

[5] S. Takeuchi, T. Nakamura, M. Shikata, Y. Togano, Y. Kondo, J. Tsubota, T. Ozaki, A. Saito, H. Otsu, H. Wang et al., Progress of Theoretical and Experimental Physics **2019** (2019)

[6] H. Wang, H. Otsu, N. Chiga, S. Kawase, S. Takeuchi, T. Sumikama, S. Koyama, H. Sakurai, Y. Watanabe, S. Nakayama et al., Communications Physics **2**, 2399 (2019)

[7] T. Kubo, D. Kameda, H. Suzuki, N. Fukuda, H. Takeda, Y. Yanagisawa, M. Ohtake, K. Kusaka, K. Yoshida, N. Inabe et al., Progress of Theoretical and Experimental Physics **2012** (2012)

[8] N. Fukuda, T. Kubo, T. Ohnishi, N. Inabe, H. Takeda, D. Kameda, H. Suzuki, Nuclear Instruments and Methods in Physics Research Section B: Beam Interactions with Materials and Atoms **317, Part B**, 323 (2013)

[9] T. Sato, Y. Iwamoto, S. Hashimoto, T. Ogawa, T. Furuta, S. Abe, T. Kai, P.E. Tsai, N. Matsuda, H. Iwase et al., Journal of Nuclear Science and Technology **55**, 684 (2018)

[10] Y. Iwamoto, T. Sato, S. Hashimoto, T. Ogawa, T. Furuta, S. Abe, T. Kai, N. Matsuda, R. Hosoyamada, K. Niita, Journal of Nuclear Science and Technology **54**, 617 (2017)

[11] A. Boudard, J. Cugnon, J.C. David, S. Leray, D. Mancusi, Phys. Rev. C **87**, 014606 (2013)

[12] S. Furihata, Nuclear Instruments and Methods in Physics Research Section B: Beam Interactions with Materials and Atoms **171**, 251 (2000)